Available online at www.sciencedirect.com
SCIENCE DIRECT®
Journal of Power Sources 140 (2005) 355–360
JOURNAL OF POWER SOURCES
www.elsevier.com/locate/jpowsour

Short communication

Structural and electrochemical properties of $Li_{1+x}Ni_{0.5}Mn_{0.5}O_{2+\delta}$ ($0 \leq x \leq 0.7$) cathode materials for lithium-ion batteries

Sun Hee Choi[a], O.A. Shlyakhtin[b], Joosun Kim[a], Young Soo Yoon[c,*]

[a] *Nano-Materials Research Center, Korea Institute of Science and Technology, P.O. Box 131, Cheongryang, Seoul 130-650, Republic of Korea*
[b] *Institute of Chemical Physics, Russian Academy of Sciences, 117334 Moscow, Russia*
[c] *Department of Advanced Technology Fusion (Center for Emerging Wireless Power Transmission Technology), Konkuk University, 1 Hwayang-dong, Gwangjin-gu, Seoul 143-701, Republic of Korea*

Received 3 July 2004; accepted 29 July 2004
Available online 18 October 2004

Abstract

A comparative analysis of the properties of $LiNi_{0.5}Mn_{0.5}O_2$ and $Li_{1+x}Ni_{0.5}Mn_{0.5}O_2$ ($0.2 \leq x \leq 0.7$) powders, obtained by the freeze drying method, was performed. Lattice parameters of $Li_{1+x}Ni_{0.5}Mn_{0.5}O_2$ decreased considerably with growing amounts of Li until $x = 0.3$; at $x > 0.5$ trace amounts of Li_2MnO_3 are observed by X-ray diffraction (XRD) patterns. X-ray photoelectron spectroscopy (XPS) analysis displayed an increase of Ni^{3+}/Ni^{2+} ratio at $0.3 < x < 0.5$, while Mn 2p spectra were almost identical in all samples. Rechargeable capacity values (V = 2.5–4.6 V) increased systematically with x reaching its maximum (185–190 mAh g^{-1}) at $x = 0.5$. Samples with superstoichiometric lithium content also demonstrated good C rate characteristics.

Keywords: Secondary Li batteries; Li–Ni–Mn oxides; Cation stoichiometry; Freeze drying; Capacity fade

1. Introduction

Due to high costs and insufficient capacity of $LiCoO_2$, commonly used as a cathode material in Li-ion batteries, much effort has been dedicated to developing cheaper alternatives. Initially, $LiNiO_2$ and $LiMnO_2$ have been studied [1–3] but stoichiometric $LiNiO_2$ demands a complicated synthesis procedure while its multi-phase reactions during electrochemical cycling leads to structural degradation [1,2]. Layered $LiMnO_2$ has a significant disadvantage in its crystallographic transformation to spinel structure, during electrochemical cycling [4,5]. To overcome the disadvantages in $LiNiO_2$, the substitution of Al [6] or Fe [7] for Ni has been investigated. Ammundsen et al. [8] have reported Al and Cr-doped monoclinic $LiMnO_2$ which showed sloping discharge curves from 4 to 2.5 V, with rechargeable capacity of more than 150 mAh g^{-1}.

Recently, a concept of a solid solution of $LiNiO_2$ and $LiMnO_2$, $Li(Ni_{0.5}Mn_{0.5})O_2$, was proposed by Ohzuku and Makimura [9], to overcome the disadvantages of $LiNiO_2$ and $LiMnO_2$. $Li(Ni_{0.5}Mn_{0.5})O_2$ has been reported as having the hexagonal O_3 structure similar to α-$NaFeO_2$ and $LiCoO_2$ [10,11]. The alternating-layer arrangement provides a very suitable two-dimensional conduction pathway for the Li^+ ions.

Most solid solutions in the Li–Ni–Mn–O system demonstrate several general features. First of all, it is relatively easy to substitute Li for Ni and Ni for Li in both A and B-positions of a hexagonal layered ABO_2 structure, due to the small difference in ionic radii between Li^+ and Ni^{2+} [12,13]. Ni ions placed at the Li position obstruct the two-dimensional diffusion of Li^+ ions and irreversible capacity fade during the initial charge.

In the case of $LiCoO_2$, Levasseur et al. [14] first reported the existence of Co^{2+} and oxygen defects in Li_xCoO_2 ($x > 1$), using Li [7] nuclear magnetic resonance and neutron diffraction measurements. It was also found that monoclinic dis-

* Corresponding author. Tel.: +82 2 2049 6042; fax: +82 2 452 5558.
E-mail address: ysyoon@konkuk.ac.kr (Y.S. Yoon).

0378-7753/$ – see front matter © 2004 Elsevier B.V. All rights reserved.
doi:10.1016/j.jpowsour.2004.07.036

tortion for $Li_{0.5}CoO_2$, during charge, can be prevented by adding extra lithium during synthesis [14,15]. Recent studies have also demonstrated the existence of single phase compounds, $Li[Ni_xLi_{(1/3-2x/3)}Mn_{(2/3-x/3)}]O_2$, with hexagonal structures which can be considered as solid solutions of $LiNiO_2$ and Li_2MnO_3 [16–19]. Such compounds contain considerable amounts of lithium in B-positions of the ABO_2 lattice and demonstrate enhanced electrochemical performance. At the same time, the properties of $LiNi_{0.5}Mn_{0.5}O_2$-based compositions, containing superstoichiometric amounts of lithium, have not been studied until now.

2. Procedure

$Li_{1+x}Ni_{0.5}Mn_{0.5}O_{2+\delta}$ (x = 0, 0.2, 0.3, 0.5, and 0.7) powder was prepared by the freeze drying method. Li acetate, Ni and Mn acetates were dissolved in water, in the stoichiometric ratio. The solution was frozen by liquid nitrogen spray, via a pneumatic nozzle, and freeze-dried at $P = 5 \times 10^{-2}$ mBar (Alpha 2–4, Christ) for 1–2 days. Thermal decomposition of precursor powders was obtained by the fast-heating of precursors to 500 °C, followed by 8 h of dwell time. The products of thermal decomposition were pressed into pellets and placed, for 12 h, into a muffle furnace preheated to 900 °C. The cooling of samples was performed by air quenching. $Li_{1+x}Ni_{0.5}Mn_{0.5}O_{2+\delta}$ powder was obtained by grinding the quenched pellets.

X-ray diffraction (XRD; Geigerflex, Rigaku, Cu Kα) measurements were conducted in the range of diffraction angles from (2θ) 17–90° at 0.5° min^{-1}. Silicon powder was used as an internal standard. The XRD patterns were indexed and lattice parameters were determined using least squares hexagonal fitting of all the diffraction lines. For X-ray photoelectron spectroscopy (XPS, PHI-5800), samples were spread over a polymeric adhesive tape and affixed to the sample holder. All spectra were recorded using an X-ray source (Al Kα radiation) with a scan range of 1400–0 eV of binding energy. The collected high-resolution XPS spectra were analyzed using an XPS peak software-fitting program. The energy scale was adjusted on the carbon peak in C1s spectra, at 284.6 eV. The micromorphology and crystallographic structure of powder particles were examined with a transmission electron microscope (TEM, Philips CM-30, U = 200 kV).

Electrochemical characterizations were obtained using a CR2032 coin-type cell with the following parameters: cut-off voltage 2.5–4.6 V and I = 5 mA g^{-1} (0.03C), 25 mA g^{-1} (0.15C), and 50 mA g^{-1} (0.3C) at room temperature. The cathode was fabricated with 20 mg of accurately weighed active material ($Li_{1+x}Ni_{0.5}Mn_{0.5}O_{2+\delta}$) and 12 mg of conductive binder (8 mg of teflonized acetylene black (TAB) and 4 mg graphite). It was pressed on 200 mm [2] of stainless steel mesh, used as the current collector, under 300 kg cm^{-2} of pressure and dried at 120 °C for 24 h in a vacuum oven. The test cell was made of a cathode and an anode (lithium metal), separated by a porous polypropylene film (Celgard 3401). The electrolyte used was a mixture of 1 M $LiPF_6$-ethylene carbonate (EC) and dimethyl carbonate (DMC) (1:1 by vol., Merck).

3. Results and discussion

XRD patterns of the synthesized powder, $Li_{1+x}Ni_{0.5}Mn_{0.5}O_{2+\delta}$, is shown in Fig. 1. The value "x" refers to the amount of superstoichiometric lithium in $Li_{1+x}Ni_{0.5}Mn_{0.5}O_{2+\delta}$. The samples in the range of $0 < x < 0.3$ are single phase, with hexagonal structures of α-$NaFeO_2$-type (space group $R\bar{3}m$), similar to a high temperature polymorph of $LiCoO_2$. Small additional peaks at 20–25°, which appeared at x = 0.5 and 0.7, can be attributed to superstructure in hexagonal ABO_2 lattice [12] or to the Li_2MnO_3 [17]. In the last case, the appearance of Li_2MnO_3 could have been caused by the exceeding of the solid solution limit of $Li_{1+x}Ni_{0.5}Mn_{0.5}O_{2+\delta}$ at $x \geq 0.5$.

This conclusion correlates quite well with the lattice parameters plots versus the amount of superstoichiometric lithium (Fig. 2), demonstrating a considerable decrease of c, up to $x = 0.3$, with little or no further changes. The character of the lattice parameters variation with x, can also be seen at the

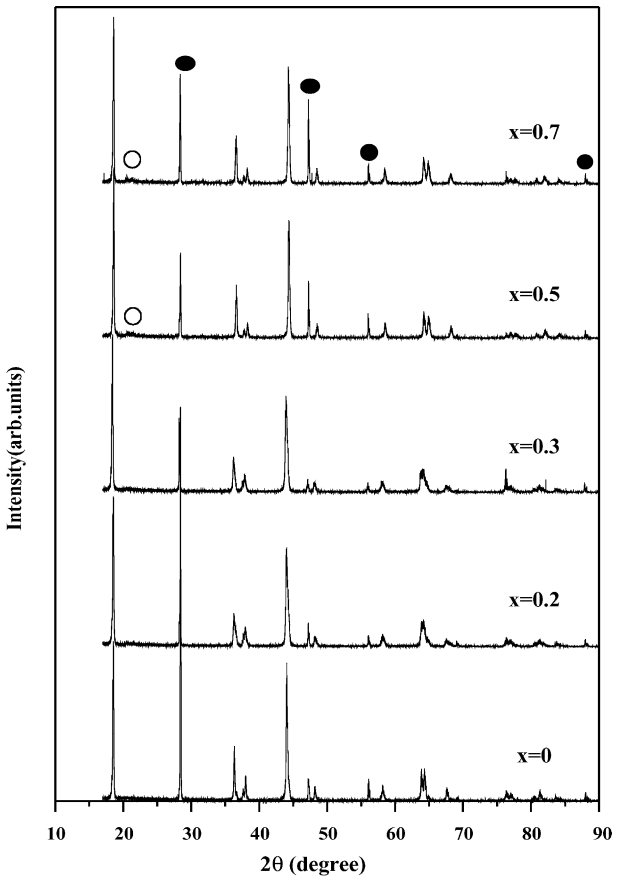

Fig. 1. XRD diffraction patterns of $Li_{1+x}Ni_{0.5}Mn_{0.5}O_{2+\delta}$ (x = 0, 0.2, 0.3, 0.5, and 0.7). The closed circles indicate Si internal standard, and the open circles indicate Li_2MnO_3.

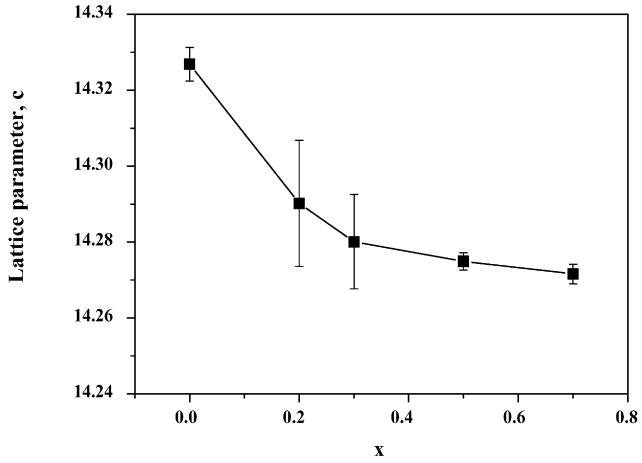

Fig. 2. Lattice parameter changes along *c*-axis plotted against superstoichiometric Li content, *x*.

formation of solid solution, until $x = 0.3$–0.5. Similar contraction of the lattice parameters, at growing Li content, was also observed in $Li[Ni_xLi_{(1/3-2x/3)}Mn_{(2/3-x/3)}]O_2$, where a variable part of lithium is allocated in B-positions, even though in that case the variation of the Li amount is accompanied by the corresponding variation of the Ni/Mn ratio. The decrease of the lattice parameters is attributed to the appearance of oxygen defects [15] and smaller radii of Ni^{3+} ions compared to Ni^{2+}. Taking into account these considerations, the systematic decrease of $Li_{1+x}Ni_{0.5}Mn_{0.5}O_{2+\delta}$ lattice parameters with *x* indicates that the allocation of extra lithium, in regular positions of ABO_2 lattice, and the composition of $Li_{1+x}Ni_{0.5}Mn_{0.5}O_{2+\delta}$ within the solid solution limit, would be more correctly interpreted as $Li[Li_{x/(2+x)}Ni_{1/(2+x)}Mn_{1/(2+x)}]O_{2-\delta}$.

In addition to lattice parameters, dependence of Ni valence states on *x* demonstrates more complex behavior. Allocation of extra lithium in regular positions of ABO_2 lattice, at minor oxygen nonstoichiometry, should be accompanied by the corresponding increase of Ni or Mn oxidation states. At the same, time XPS peaks indicate that the centers of Ni $2p_{3/2}$ peaks (854.9 eV) show little or no shift to higher energies until $x = 0.5$ (Fig. 3A). The observed value of binding energy for $0 \leq x \leq 0.3$ is higher than was reported by Kang et al. [20] (854.3 eV); this can be attributed to the presence of Ni in both 2+ and 3+ valence states. For $x = 0.5$ and 0.7, the Ni $2p_{3/2}$ peak shifts to 855.4 eV and could be assigned to Ni^{3+}. The presence of the satellite peaks has also been observed by other researchers and has been ascribed to the multiple splitting of the nickel oxide energy level [21,22].

However, the Mn 2p spectra of the samples with stoichiometric and superstoichiometric amounts of lithium are very similar (Fig. 3B). Specifically, until $x = 0.3$, the Mn $2p_{3/2}$ peak is observed at 642.5 eV, demonstrating good correlation with the value (642.4 eV) reported by Kang et al. [20]. At $x = 0.5$ and 0.7, the Mn $2p_{3/2}$ peak is shifted slightly to 642.7 eV, even though both values are rather typical for Mn^{4+} oxides [23]. It can be concluded that the oxidation state of Mn is maintained at 4+ regardless of Li content and the charge

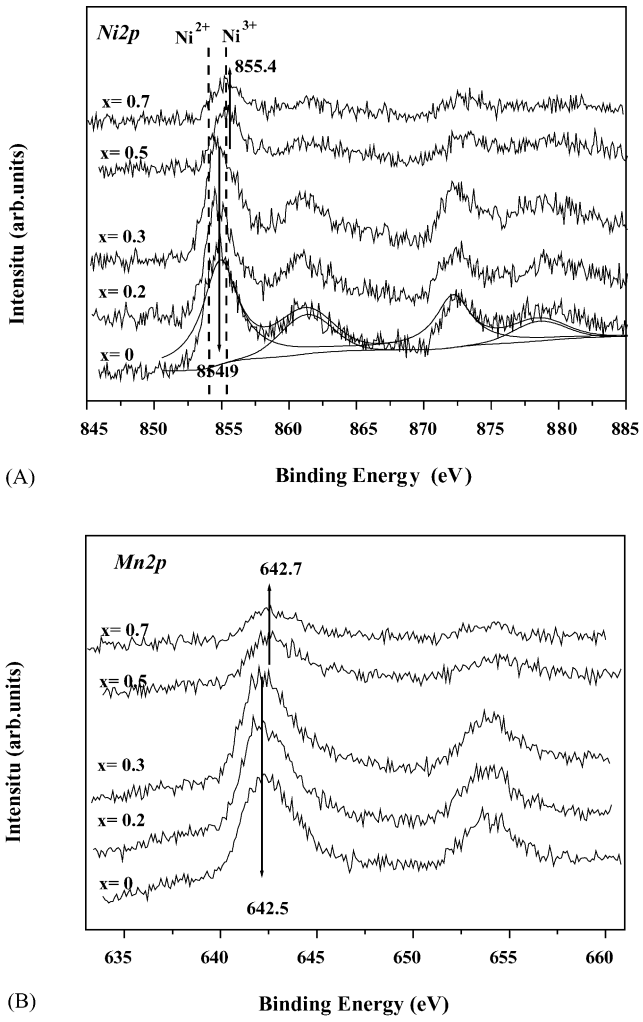

Fig. 3. XPS spectra of Ni $2p_{3/2}$ (A) and Mn $2p_{3/2}$ (B) of the synthesized $Li_{1+x}Ni_{0.5}Mn_{0.5}O_{2+\delta}$ powders.

compensation mechanism concerns mostly the Ni oxidation states.

Most parts of the electron diffraction patterns of $Li_{1+x}Ni_{0.5}Mn_{0.5}O_{2+\delta}$ powders, recorded along the [0 0 0 1] zone axis, are also normal for the well-ordered hexagonal structure of α-$NaFeO_2$-type (Fig. 4A). The major spots correspond to the $\{1\,1\,\bar{2}\,0\}$ reflections. The increase of the amount of lithium in $Li_{1+x}Ni_{0.5}Mn_{0.5}O_{2+\delta}$ is accompanied by the appearance of the cubic spinel phase (Fig. 4B and C, arrows). Similar patterns, observed after continuous cycling of $LiCoO_2$ cathodes [24], were attributed to the formation of spinel structures, due to the cation disorder in the hexagonal lattice of $LiCoO_2$. In our study, the cation disorder could be caused by complicated long-range ordering in samples with $x > 0$ [25]. However, the amount of the cubic phase remains rather small, even at large *x* values.

Fig. 5A shows the cycle performance of $Li_{1+x}Ni_{0.5}Mn_{0.5}O_{2+\delta}$-based cathode materials at 0.1 mA. The reversible discharge capacity demonstrates a clear dependence on Li content, systematically increasing with *x*

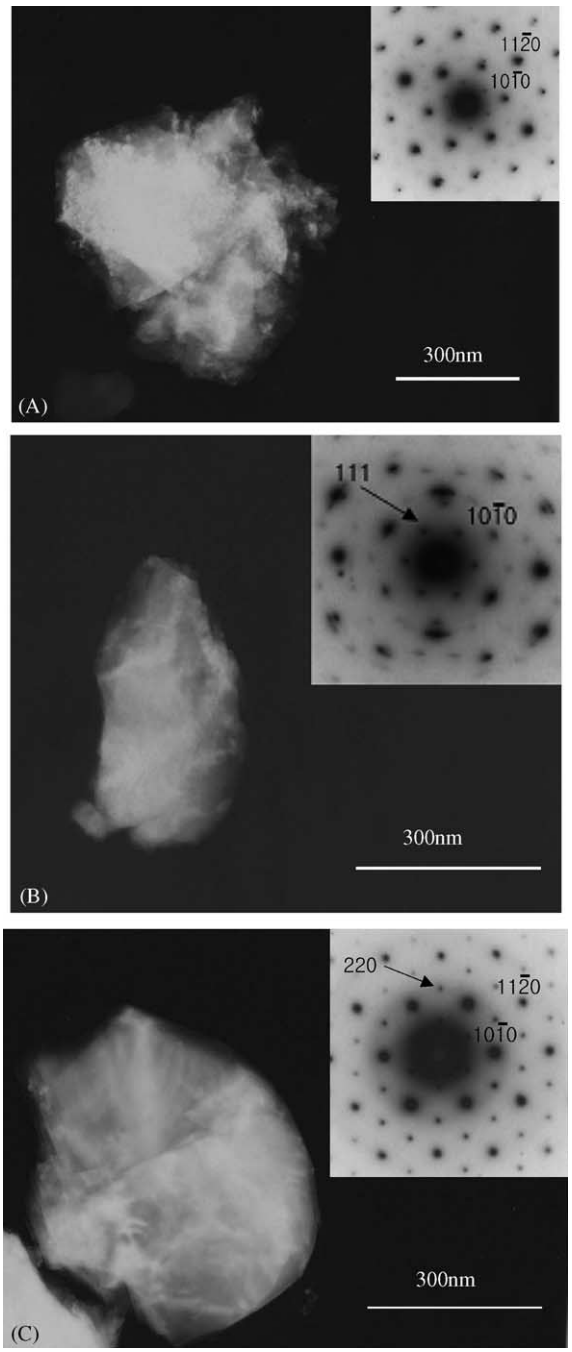

Fig. 4. Bright field TEM and selected area electron diffraction (SAED) patterns of the $Li_{1+x}Ni_{0.5}Mn_{0.5}O_{2+\delta}$ powders: (A) $x = 0$; (B) $x = 0.3$, and (c) $x = 0.7$.

up to $x = 0.5$. The enhancement of capacity values, caused by superstoichiometric lithium, is especially significant at $x = 0.2$, compared to stoichiometric samples ($x = 0$). *C* rate characteristics of cathodes with extra lithium are also considerably better than the parameters of stoichiometric $LiNi_{0.5}Mn_{0.5}O_{2+\delta}$ cathodes after 25 cycles (Fig. 5B).

Assuming that additional lithium atoms are placed in the regular positions of the hexagonal lattice, the observed increase of capacity values can be explained by the suppression of antisite defects in A-positions (Ni/Li exchange) and, hence, the promotion of Li transport via A-positions. This effect was found in $Li[Ni_xLi_{(1/3-2x/3)}Mn_{(2/3-x/3)}]O_2$ by the Rietveld analysis of diffraction patterns [12].

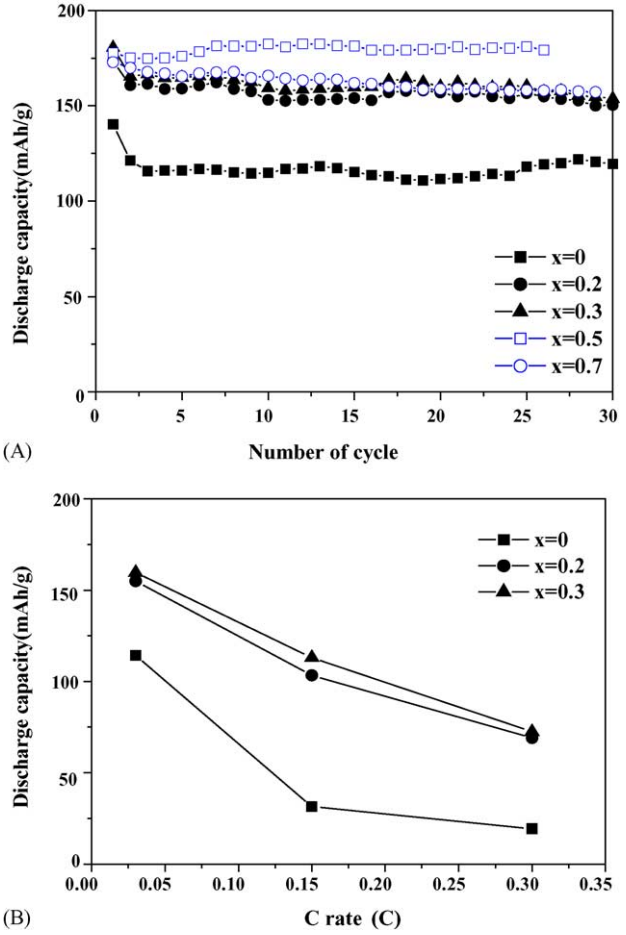

Fig. 5. Cycle behavior of $Li_{1+x}Ni_{0.5}Mn_{0.5}O_{2+\delta}$ powders ($x = 0$, 0.2, 0.3, 0.5, and 0.7) at $I = 0.1$ mA (0.03*C*) (A); and *C* rate characteristics of $Li_{1+x}Ni_{0.5}Mn_{0.5}O_{2+\delta}$ powders ($x = 0$, 0.2, and 0.3) after 25 cycles (B).

Meanwhile, stepwise capacity gain at $x = 0.5$ can be caused by other reasons. Fig. 6 shows differential capacity curves of $Li_{1+x}Ni_{0.5}Mn_{0.5}O_{2+\delta}$ powders at 0.1 mA during first cycle. For samples with $x \geq 0.5$, the appearance of irreversible peaks at around 4.5 V was observed in the first charge profile (Fig. 6C and D). Similar peaks, at slightly higher voltage (4.6 V), were observed during the first charge of $Li[Ni_xLi_{(1/3-2x/3)}Mn_{(2/3-x/3)}]O_2$ cathodes, up to 4.8 V [12]. The intensity of these peaks, attributed by the authors to the simultaneous extraction of both Li and O during the first charge, followed by the formation of more perfect structures during following discharge, was roughly proportional to the capacity increase in cathode materials with different *x* values during further cycling. The nature of 4.5 V peaks in $Li_{1+x}Ni_{0.5}Mn_{0.5}O_{2+\delta}$ needs more detailed, further investigation, but merely the fact of their appearance indicates a considerable difference in the character of Li intercalation processes at $x \geq 0.5$.

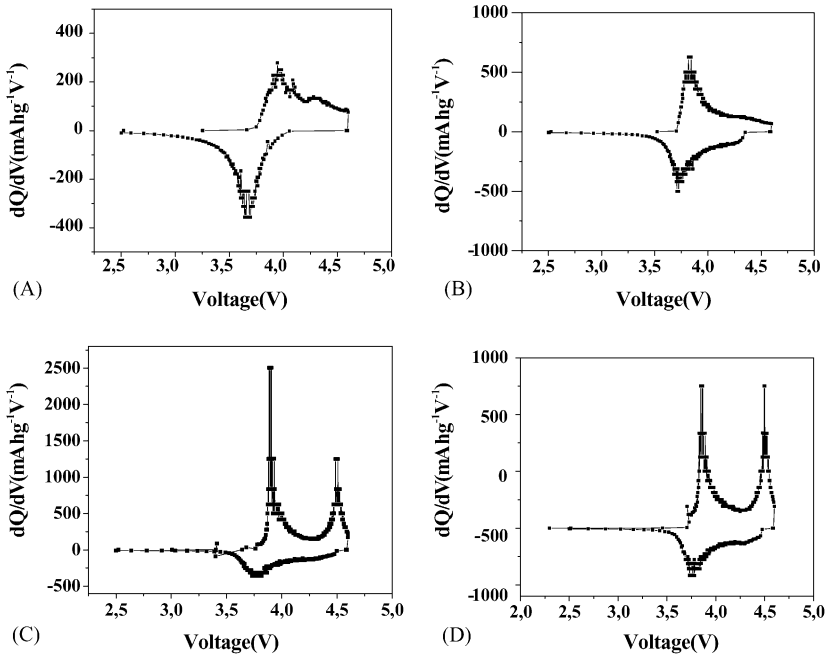

Fig. 6. Differential capacity vs. voltage curves of $Li_{1+x}Ni_{0.5}Mn_{0.5}O_{2+\delta}$ powders during first cycle: (A) $x = 0$, (B) $x = 0.3$, (C) $x = 0.5$, and (D) $x = 0.7$ at $I = 0.1$ mA.

The discharge capacity decrease, at $x = 0.7$ (Fig. 5A), can be more simply explained. According to Fig. 3A, the amount of Ni^{3+} at $x = 0.7$ is not higher than at $x = 0.5$, therefore that lack of Ni^{2+} cannot be the cause of this fall in capacity. At the same time, Figs. 1 and 2 demonstrates that the increase of Li content in the starting mixture, at $x \geq 0.5$, is not accompanied by its appearance in the regular positions of hexagonal $Li_{1+x}Ni_{0.5}Mn_{0.5}O_{2+\delta}$ lattice—probably due to the formation of electrochemically inactive Li_2MnO_3. Taking into account that electrochemical capacity is calculated per 1 cm^2 of cathode or per 1 g of the whole cathode mass, whether electrochemically active or not, an increase of x beyond the solid solution limit should be accompanied by a systematic decrease of the actual amount in of cyclable phase, in 1 g of cathode mass. This conclusion correlates quite well with the capacity measurement results, so that further increments of x should be accompanied by a decline of the electrochemical performance of cathode material.

4. Conclusion

The experiments which we performed, demonstrate that electrochemical properties of $Li_{1+x}Ni_{0.5}Mn_{0.5}O_{2+\delta}$ are substantially controlled by Li stoichiometry. Similar to $Li[Ni_xLi_{(1/3-2x/3)}Mn_{(2/3-x/3)}]O_2$-based materials with variable Ni/Mn ratio, $Li_{1+x}Ni_{0.5}Mn_{0.5}O_{2+\delta}$ samples with $0 < x \leq 0.5$ also demonstrate considerably higher capacity values and better cycle performance than $LiNi_{0.5}Mn_{0.5}O_2$. More detailed structural investigation of $Li_{1+x}Ni_{0.5}Mn_{0.5}O_{2+\delta}$ is needed, while preliminary analysis by XRD and XPS methods shows the formation of a solid solution with a layered hexagonal structure at $0 \leq x \leq 0.3$–0.4 with Li placed in regular positions of the hexagonal lattice. The oxidation state of Mn proved constant (4+) for all samples in this study, while the oxidation state of Ni increased from 2+ to 3+. Exceeding the solid solution limit resulted in the detection of Li_2MnO_3 at $x = 0.5$. Any further increase in lithium content was accompanied by reversible capacity decrease.

Acknowledgement

We would like to show our appreciation for the support of National Research Laboratory Program (Development of monolithic high power hybrid battery) of the Ministry of Science and Technology, Republic of Korea.

References

[1] I. Davidson, J.E. Greedan, U. von Sacken, C.A. Michal, J.R. Dahn, Solid State Ionics 46 (1991) 243.
[2] G. Dutta, A. Manthiram, J.B. Goodenough, J. Solid State Chem. 96 (1992) 123.
[3] T. Ohzuku, A. Ueda, M. Nagayama, Y. Iwakoshi, H. Komori, Electrochim. Acta 38 (1993) 1159.
[4] G. Vitins, K. West, J. Electrochem. Soc. 144 (1997) 2587.
[5] Y.I. Jang, B. Huang, Y.M. Chiang, D.R. Sadoway, Electrochem. Solid-State Lett. 1 (1998) 13.
[6] Q. Zhong, U. von Sacken, J. Power Sources 54 (1995) 221.
[7] J.N. Reimers, E. Rossen, C.D. Jones, J.R. Dahn, Solid State Ionics 61 (1993) 335.
[8] B. Ammundsen, J. Desilvestro, R. Steiner, P. Pickering, Proceedings of the 10th International Meeting on Lithium Batteries, Como, May 2000, Abstract No. 17.

[9] T. Ohzuku, Y. Makimura, Chem. Lett. 744 (2001).
[10] J. Akimoto, Y. Gotoh, Y. Oosawa, J. Solid State Chem. 141 (1998) 298.
[11] L.D. Dyer, B.S. Borie Jr., G.P. Smith, J. Am. Chem. Soc. 76 (1954) 1499.
[12] Z. Lu, L.Y. Beaulieu, R.A. Donaberger, C.L. Thomas, J.R. Dahn, J. Electrochem. Soc. 149 (2002).
[13] R. Stoyanova, E. Zhecheva, R. Alcantara, J.L. Tirado, G. Bromiley, F. Bromiley, T. Boffa Balaran, Solid State Ionics 161 (2003) 197.
[14] S. Levasseur, M. Menetrier, E. Suard, C. Delmas, Solid State Ionics 128 (2000) 11.
[15] N. Imanishi, M. Fujii, A. Hirano, Y. Takeda, M. Inaba, Z. Ogumi, Solid State Ionics 140 (2001) 45.
[16] Z. Lu, D.D. MacNeil, J.R. Dahn, Electrochem. Solid State 4 (2001) 191.
[17] S.S. Shin, Y.K. Sun, K. Amine, J. Power Sources 112 (2002) 634.
[18] Z. Lu, J.R. Dahn, J. Electrochem. Soc. 149 (2002) 815.
[19] Y.J. Park, M.G. Kim, Y.S. Hong, X. Wu, K.S. Ryu, S.H. Chang, Solid State Commun. 127 (2003) 509.
[20] S.H. Kang, J. Kim, M.E. Stoll, D. Abraham, Y.K. Sun, K. Amine, J. Power Sources 112 (2002) 41.
[21] A.F. Carley, S.D. Jackson, J.N. O'shea, M.W. Roberts, Surf. Sci. 440 (1999) 868.
[22] K. Amine, H. Tukamoto, H. Yasuda, Y. Fujita, J. Electrochem. Soc. 143 (1996) 1607.
[23] K.M. Shaju, G.V. Subba Rao, B.V.R. Chowdari, Electrochim. Acta 48 (2003) 1505.
[24] H. Gabrisch, R. Yazami, B. Fultz, J. Power Sources 119–121 (2003) 674.
[25] O.A. Shlyakhtin, Y.J. Oh, Y.S. Yoon, Proceedings of the First International Conference on Polymer Batteries and Fuel Cells, Jeju, Korea, June 2003, Abstract No. TU-100.